

ADVANCED BIPED GAIT GENERATOR USING NARX-MLP NEURAL MODEL OPTIMIZED BY ENHANCED EVOLUTIONARY ALGORITHM

Tran Thien Huan¹ , Ho Pham Huy Anh^{2,3,*} 

¹*Faculty of Applied Sciences (FAS), HCM City University of Technology and Education (HCMUTE), Ho Chi Minh City, Vietnam*

²*Faculty of Electrical-Electronics Engineering (EEEE), Ho Chi Minh City University of Technology (HCMUT), 268 Ly Thuong Kiet Street, District 10, Ho Chi Minh City, Vietnam*

³*Vietnam National University Ho Chi Minh City (VNU-HCM), Linh Trung Ward, Thu Duc City, Ho Chi Minh City, Vietnam*

*E-mail: hphanh@hcmut.edu.vn

Received: 19 June 2022 / Published online: 30 September 2022

Abstract. A novel biped walking pattern combining robust zero-moment-point ZMP technique and pre-determined foot-lifting value is proposed in this paper. The implementation of suggested approach contains following stages. Initially, a one-step ZMP curve for a small-sized humanoid is created using the 3rd-order interpolating equation, with pre-determined velocity responding the ZMP concept. The next step, biped gait planning is modeled as a non-linear MIMO plant including ten degree-of-freedom DOF. Then, the installation of a biped walking pattern generator (WPG) based on the new hybrid Neural-NARX model is completed. Eventually, the novel Enhanced Differential Evolution (EDE) technique is applied to optimally identify the weights of the hybrid Neural-NARX structure, for ensuring robust robot walking in terms of desired ZMP trajectories and pre-determined foot-lifting value. All case studies confirm that it is surely provide a biped WPG satisfying both of the effectiveness and high robustness. The verification of the newly proposed WPG is adequately tested via both simulation and experiment results.

Keywords: small-sized biped, walking pattern generator (WPG), Nonlinear Auto-Regressive eXogenous (NARX) model, model, Enhanced Differential Evolution (EDE) optimization technique, zero-moment-point (ZMP) concept.

1. INTRODUCTION

The ZMP principle has been firstly applied to humanoid gait planning by Vukobratovic which represents relation from humanoid joint-angular values with the ZMP which is able to be expressed as a differential equation. It is necessary to note that it is strongly difficult to generate trajectorial curves of humanoid joint-angular values that ensure the

real ZMP perfectly following the desired ZMP curve due to its quite non-linearity. To surpass that disadvantage, the complicated ZMP functions are simply transformed via transformations appropriate. Such as, authors in [1, 2] suggested a forecast adjustment based on an inverse pendubot structure. Oshahi et al. in [3] introduced a novel ZMP-based WPG successfully applied to biped. Different from the techniques above-mentioned, Yi et al. in [4] introduced a new model from which important requirements were conditioned as to ensure biped to stably walking on uneven ground. Improving the resulted humanoid joint-angular curves, a humanoid WPG generator is innovatively proposed via choosing the optimal parameters as to guarantee the humanoid robust walking.

Several research approaches also investigated the humanoid WPG as an optimal problem regarding to numerous trade-off requirements. In detail it relates to optimum evolutionary algorithms which played an important role to biped development in terms of effectiveness in energy-consumed cost and biped stepping robustness by optimizing biped parameters. Such as, Liu et al. in [5] applied a new dynamic walking control for biped robots linking linear inverted pendulum mode with biped coefficient optimization. Authors in [6] (2021) introduced a novel optimization approach for humanoid robot motion planning. Meng et al. [7] proposed an accelerating proximal policy optimization on CPU-FPGA applied to biped stable walking. Huan et al. in [8] suggested an adaptive gait generation for biped robot based on evolutionary neural-model optimized with MDE optimization technique. Van-Huan et al. in [9] successfully applied an optimal trajectory generation for biped robust walking, among them. However, in order to catch humanoid gaits, biped robots have to control their hip-shift.

Recently, deep machine learning techniques applied to biped robot have been increasingly attracted the investigation of numerous researchers. Wang et al. [10] initiatively applied machine learning algorithms in bipedal robot walking control. Phaniteja et al. [11] suggested a deep reinforcement learning method for dynamically stable inverse kinematics of biped robot. Authors in [12] introduced a real-world reinforcement learning for autonomous biped robot docking. Hwang et al. [13] proposed a new motion segmentation and balancing technique for biped robot's imitation learning. Kim et al. in [14] introduced an innovative push recovery control for biped robot using reinforcement learning technique, and so on. Especially, several neural-based learning approaches also initiatively suggested as to biped stably walking control. Gil et al. in [15] introduced a new deep learning approach for efficient biped gait generation using reinforcement learning and artificial neural networks. Xi and Chen [16] proposed a new biped walking control on static and rotating platforms using hybrid neural-based reinforcement learning method. Zhang et al. [17] (2022) successfully applied a new neural reinforcement learning framework for biped gait control. The disadvantage of these deep learning techniques relates to the fact that the learning methods show too complicated that they seem hard to be applied in practical humanoid applications.

Based on biped WPG results above-mentioned, a novel biped WPG technique (using NARXMLP neural model optimized by enhanced evolutionary algorithm) is suggested satisfying both of desired ZMP trajectories and pre-determined foot-lifting value. The design steps of that suggested technique includes as. Firstly, a desired one-step ZMP

curve for biped is developed using the 3rd-order interpolation function. Second, it optimally identifies the biped walking process via a nonlinear 10 DoF system. Third, a novel biped WPG model based on the hybrid Neural-NARX is created. Concerning the proposed Neural-NARX model, it consists of 2 inputs related to the co-ordinate of desired ZMP value at $t(k)$ and 2 related to the coordinate data of the real ZMP point at $t(k - 1)$. Then Neural-NARX model generates 4 outputs related to biped gait generating parameters. Eventually, the new Enhanced Differential Evolution (EDE) optimization method is applied to optimally identify the weighting values of the Neural-NARX scheme, as to guarantee robust robot walking satisfying both of desired ZMP trajectories and pre-chosen foot-lifting value.

This paper includes following sections. Section 2 introduces the novel humanoid WPG generator. Section 3 suggests the new enhanced EDE algorithm for optimum estimating the weights of the proposed humanoid Neural-NARX structure. Descriptions and analysis contributed to the simulation plus experiment results will be presented in Section 4. Finally, conclusions belong to Section 5.

2. BIPED WPG GENERATOR

Fig. 1 presents the block diagram of the suggested robust humanoid WPG generator using the novel Neural-NARX model. The WPG is implemented using resulted basis introduced at [18]. The proposed hybrid Neural-NARX model used for regulating WPG generator is initiatively implemented. Fig. 1 clarifies that the Neural-NARX model outputs play the role of inputs of WPG which generates the 10 rotating angular values for ensuring the humanoid stably walking. The output sent-back of humanoid composes of x, y coordinates of ZMP magnitude. Those 2 parameters provided to NARX model with desired ZMP values, which then generates the four principal parameters ($\varphi_1(k), \dots, \varphi_4(k)$)

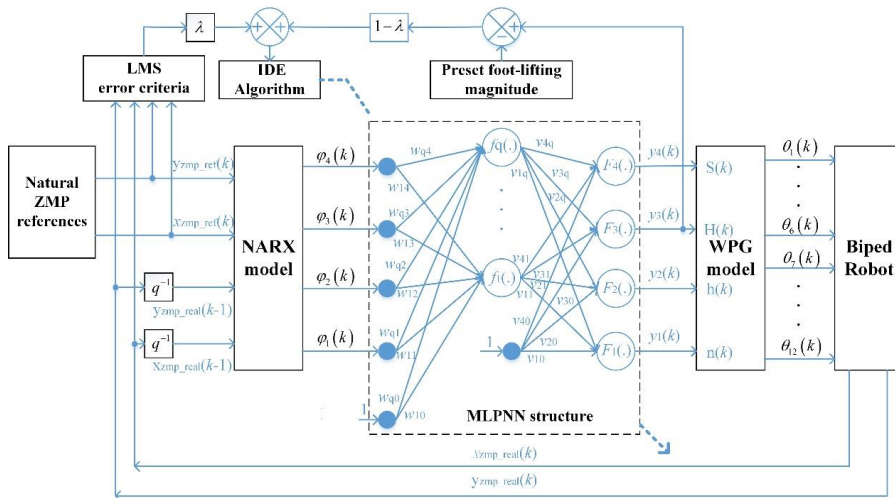


Fig. 1. Block diagram of suggested robust humanoid WPG generator using the novel Neural-NARX model

sent to Neural MLPNN model. The coefficients of proposed biped Neural-NARX model are to be optimum estimated using the Enhanced Differential Evolution (EDE) optimization approach.

2.1. Real ZMP trajectories of Humanoid Robot

Regarding biped walking, ZMP trajectory lies below the support-foot. Then, man proves easy to walk smoothly regarding to flexible speed. Fig. 2 shows that the curve of $p_1 p_2 p_3 p_4$ forms the human ZMP trajectory within one step. It is clear to note that A, B, and C represent the support-feet centres. Within the 1st DSP, $p_1 - p_2$ represents the distance that ZMP moved. In SSP Phase, the ZMP curve contains p_2 to p_3 . In DSP phase, this curve contains p_3 to p_4 .

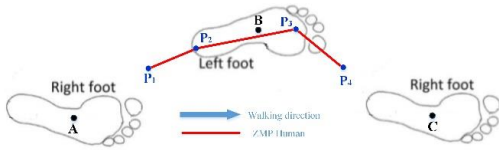


Fig. 2. ZMP shift description

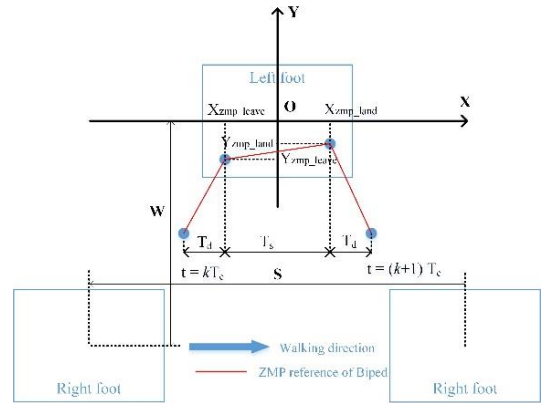


Fig. 3. Biped real ZMP trajectory

Then the real biped ZMP trajectory is able to be attained using those constraints. Assuming that the 1-step period equals T_c , hence biped k^{th} period shows between kT_c to $(k + 1)T_c$, with $k = 1, 2, \dots, K$; with K denotes the biped total steps. As to clarify, we define the biped k^{th} step to begin using the right foot lifting at $t = kT_c$, and to stop during the right foot touch the surface at $t = (k + 1)T_c$. That procedure is described in Fig. 3.

Defining $(X_{zmp_leave}, Y_{zmp_leave})$ as the ZMP coordinates during the swing leg moves; $(X_{zmp_land}, Y_{zmp_land})$ represents the ZMP coordinates during the supporting leg (right leg) fixed on surface; T_d represents the DSP phase duration; T_s denotes the SSP phase duration. The co-ordinate system (Oxy) positioned at the support-foot centers (left foot). Followed constraints are derived with S represents biped step value, w denotes the length from 2 biped legs:

$$x_{zmp_ref}(t) = \begin{cases} -\frac{S}{4}, & t = kT_c \\ X_{zmp_leave}, & t = kT_c + T_d \\ X_{zmp_land}, & t = kT_c + T_d + T_s \\ \frac{S}{4}, & t = (k + 1)T_c \end{cases} \quad (1)$$

$$y_{zmp_ref}(t) = \begin{cases} -\frac{w}{2}, & t = kT_c \\ Y_{zmp_leave}, & t = kT_c + T_d \\ Y_{zmp_land}, & t = kT_c + T_d + T_s \\ -\frac{w}{2}, & t = (k+1)T_c \end{cases} \quad (2)$$

To guarantee a flat curve, it needs that not only the first derivation $\dot{x}_{zmp_ref}(t)$, $\dot{y}_{zmp_ref}(t)$, but also the 2nd derivative terms $\ddot{x}_{zmp_ref}(t)$, $\ddot{y}_{zmp_ref}(t)$ being continuous, with respect to special nodes at $t = kT_c, kT_c + T_d, kT_c + T_d + T_s$ and $(k+1)T_c$.

In order to meet with the requirements (1)–(2), and the 1st and 2nd derivatives' continual constraints above, the polynomial order required too high and thus its computation falling in difficulty if applying interpolation. To surpass these drawbacks, the desired biped ZMP trajectory will be calculated via the third-order interpolation (developed from [19]).

Thus, $x_{zmp_ref}(t)$ and $y_{zmp_ref}(t)$ will be characterized by the third-order polynomial description, and then the 2nd derivatives, $\ddot{x}_{zmp_ref}(t)$, $\ddot{y}_{zmp_ref}(t)$ available to be always continuous. By varying the values of constraint parameters $X_{zmp_leave}, Y_{zmp_leave}, X_{zmp_land}, Y_{zmp_land}, S, T_c, T_d$ and T_s , it enables to generate versatile desired biped ZMP trajectories.

2.2. Proposed WPG generator

The WPG ensures biped gait robust walking via desired ZMP trajectories. This research suggests a ten-DOF model (composing of 4 for hips, 2 for knees and 4 with ankles) shown in Fig. 4 as follows,

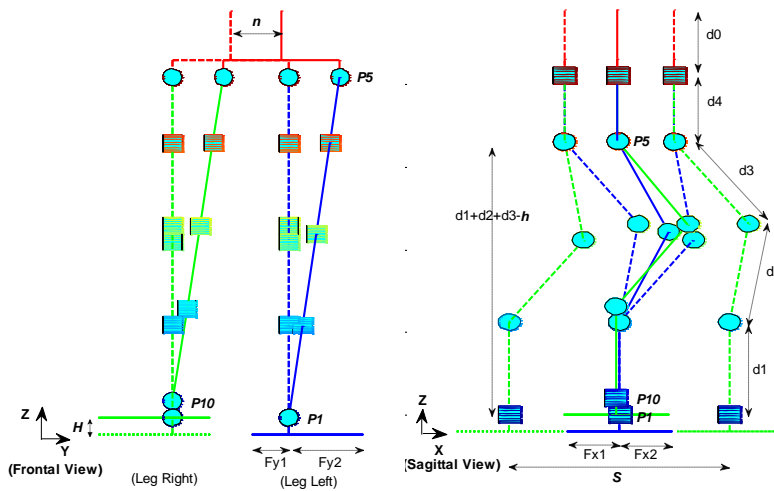


Fig. 4. Structure of a humanoid stable 1-step walking

The motions of P_1, P_5 and P_{10} are fully described in (3). In which, T_c represents humanoid 1-step duration (s), w denotes the distance between 2 legs,

$$\tau = \begin{cases} t & \text{if } 0 \leq t < T_c \\ t - T_c & \text{otherwise} \end{cases} \quad \text{and } u(t) = \begin{cases} 0 & \text{if } t < 0 \\ 1 & \text{otherwise} \end{cases} .$$

$$\left\{ \begin{array}{l} P_{1x}(t) = P_{1y}(t) = P_{1z}(t) = 0, \\ P_{5x}(t) = \frac{\mathbf{S}}{4} \sin\left(\frac{\pi}{T_c}\left(t - \frac{T_c}{2}\right)\right), \\ P_{5y}(t) = n \sin\left(\frac{\pi}{T_c}\tau\right) \cdot \left[u(\tau) - u\left(\tau - \frac{T_c}{2}\right)\right] \\ \quad + n \cos\left(\frac{\pi}{T_c}\left(\tau - \frac{T_c}{2}\right)\right) \cdot \left[u\left(\tau - \frac{T_c}{2}\right) - u(\tau - T_c)\right], \\ P_{5z}(t) = (d_1 + d_2 + d_3 - \mathbf{h}), \\ P_{10x}(t) = \frac{\mathbf{S}}{2} \sin\left(\frac{\pi}{T_c}\left(t - \frac{T_c}{2}\right)\right), \\ P_{10y}(t) = -w, \\ P_{10z}(t) = \mathbf{H} \sin\left(\pi\left(\frac{P_{10x}(t)}{\mathbf{S}}\right) + \frac{1}{2}\right), \\ \theta_1(t) = \arctan\left(\frac{y_l(t)}{z_l(t)}\right), \quad \theta_5(t) = -\theta_1(t), \\ \theta_{10}(t) = \arctan\left(\frac{y_r(t)}{z_r(t)}\right), \quad \theta_6(t) = -\theta_{10}(t), \\ \theta_3(t) = \pi - \theta_A(t), \quad \theta_8(t) = \pi - \theta_C(t), \\ \theta_4(t) = \frac{\pi}{2} - \theta_A(t) + \theta_B(t) - \arcsin\left(\frac{x_l(t)}{l_l(t)}\right), \\ \theta_7(t) = \frac{\pi}{2} - \theta_C(t) + \theta_D(t) - \arcsin\left(\frac{x_r(t)}{l_r(t)}\right), \\ \theta_2(t) = \theta_3(t) - \theta_4(t), \quad \theta_9(t) = \theta_8(t) - \theta_7(t) \end{array} \right. \quad (3)$$

$$\left. \begin{array}{l} \theta_1(t) = \arctan\left(\frac{y_l(t)}{z_l(t)}\right), \quad \theta_5(t) = -\theta_1(t), \\ \theta_{10}(t) = \arctan\left(\frac{y_r(t)}{z_r(t)}\right), \quad \theta_6(t) = -\theta_{10}(t), \\ \theta_3(t) = \pi - \theta_A(t), \quad \theta_8(t) = \pi - \theta_C(t), \\ \theta_4(t) = \frac{\pi}{2} - \theta_A(t) + \theta_B(t) - \arcsin\left(\frac{x_l(t)}{l_l(t)}\right), \\ \theta_7(t) = \frac{\pi}{2} - \theta_C(t) + \theta_D(t) - \arcsin\left(\frac{x_r(t)}{l_r(t)}\right), \\ \theta_2(t) = \theta_3(t) - \theta_4(t), \quad \theta_9(t) = \theta_8(t) - \theta_7(t) \end{array} \right\} \quad (4)$$

The mass of links is assumed to be concentrated at the joints situated at the distal points. As to clarify, the humanoid movement is considered in forward way. Using Fig. 4, it is evident to see that there are three main humanoid trajectories, namely at first the hip curve $\mathbf{P}_5 = [P_{5x}, P_{5y}, P_{5z}]$ then, second the ankle curve $\mathbf{P}_1 = [P_{1x}, P_{1y}, P_{1z}]$ of the support-leg, and eventually the ankle curve $\mathbf{P}_{10} = [P_{10x}, P_{10y}, P_{10z}]$ of the swing-leg, which were all dependent on the four key coefficients $(\mathbf{S}, \mathbf{H}, \mathbf{h}, \mathbf{n})$, as shown in Fig. 4. Hence three selected curves $\mathbf{P}_1, \mathbf{P}_5, \mathbf{P}_{10}$ can be considered as ideal sinus shape, and then completely shown as follows, (developed from [18]).

The 10 joint-angular curves located at two humanoid legs in 1-step stepping duration show possible to be expressed using only $\mathbf{P}_1 = [P_{1x}, P_{1y}, P_{1z}]$, $\mathbf{P}_5 = [P_{5x}, P_{5y}, P_{5z}]$ and $\mathbf{P}_{10} = [P_{10x}, P_{10y}, P_{10z}]$ based on the inverse trigonometric humanoid equations. Then the pseudo-kinetic technique exploiting humanoid joint-rotating values is used, and shown at (4), in which $x_l, y_l, z_l, x_r, y_r, z_r, l_l, l_r, \theta_A, \theta_B, \theta_C, \theta_D$ represent kinetic parameters of humanoid (consulted more in [18]).

The humanoid robust stepping is validated via the ZMP concept. It concludes that, if ZMP x, y coordinates situated inside support-foot surface, humanoid holds robust stepping. The ZMP x, y coordinate equations in terms of humanoid dynamics coefficients are exactly presented as follows (developed under [20]):

$$\begin{cases} x_{ZMP} = \frac{\sum_{i=1}^n m_i (\ddot{P}_{zi} + g) P_{xi} - \sum_{i=1}^n m_i \ddot{P}_{xi} P_{zi}}{\sum_{i=1}^n m_i (\ddot{P}_{zi} + g)}, \\ y_{ZMP} = \frac{\sum_{i=1}^n m_i (\ddot{P}_{zi} + g) P_{yi} - \sum_{i=1}^n m_i \ddot{P}_{yi} P_{zi}}{\sum_{i=1}^n m_i (\ddot{P}_{zi} + g)}, \end{cases} \quad (5)$$

with m_i represents the i th link mass; (P_{xi}, P_{yi}, P_{zi}) denotes the i^{th} link coordinates center; g is the gravitational acceleration; \ddot{P}_{xi} and \ddot{P}_{yi} denote the i^{th} link accelerating values in x - and y -profile; (x_{ZMP}, y_{ZMP}) represent the ZMP values. The joint position, $P_i = (P_{ix}, P_{iy}, P_{iz})$, be determined via humanoid joint-angular values $(\theta_1, \theta_2, \theta_3, \theta_4, \theta_5, \theta_6, \theta_7, \theta_8, \theta_9, \theta_{10})$ in each 1-step duration (developed under [18]). Moreover the link speed $\dot{P}_i(t)$ and acceleration $\ddot{P}_i(t)$ values can be calculated via $P_i(t)$.

2.3. Proposed Biped Neural-NARX model

The new Neural-NARX structure is suggested by combining the NARX scheme and MLP Neural model. Improving that linkage, the Neural-NARX model enhances not only the powerful approximating ability of MLP neural structure but also the perfect forecast capacity of NARX model. Moreover, the weights of Neural-NARX model will be optimized via the new EDE optimization technique.

Using Fig. 1, the MLP neural model contains a 3-layer in which $n = 4$ representing the amount of input-nodes, q representing the amount of hidden-nodes and $m = 4$ representing the amount of output-layer nodes; $\varphi(k) = [\varphi_1(k), \varphi_2(k), \varphi_3(k), \varphi_4(k)]^T$ denotes regressive values which represent delayed values of $[x_{zmp_real}(k-1), y_{zmp_real}(k-1)]$ and the desired $[x_{zmp_ref}(k), y_{zmp_ref}(k)]$ ZMP values; $y(k) = [y_1(k), y_2(k), y_3(k), y_4(k)]$ denotes the forecast output values which represent the biped four principal gait coefficients $[S(k), H(k), h(k), n(k)]$; w_{jl} is weighted value of j^{th} layer; w_{j0} represents the bias weight ($j = 1, \dots, q; l = 1, \dots, n$); v_{ij} denotes the weight of the i^{th} output layer; v_{i0} denotes the output bias weight ($i = 1, \dots, n; j = 1, \dots, q$); $f_j(\cdot)$ represents the hidden activating function ($j = 1, \dots, q$) and $F_i(\cdot)$ is the output activation function ($i = 1, \dots, n$); D represents the whole threshold magnitude of MLP neural model. Thus the forecast output will be determined as follows

$$y_i(k, \theta) = F_i \left(\sum_{j=1}^q v_{ij} f_j \left(\sum_{l=1}^{m=4} w_{jl} \varphi_l(k) + w_{j0} \right) + v_{i0} \right), \quad i = 1, \dots, n = 4. \quad (6)$$

In which, $\varphi(k)$ represents regressive values; θ denotes the weight one. Those two vectors are fully defined as,

$$\begin{aligned} \varphi(k) &= [\varphi_1(k), \varphi_2(k), \varphi_3(k), \varphi_4(k)]^T \\ &= [x_{zmp_real}(k-1), y_{zmp_real}(k-1), x_{zmp_ref}(k), y_{zmp_ref}(k)]^T, \end{aligned} \quad (7)$$

$$\begin{aligned}\theta &= [w_{jl}, w_{j0}, v_{ij}, v_{i0}]^T; \quad j = 1, \dots, q; \quad l = 1, \dots, n = 4; \quad i = 1, \dots, m = 4 \\ &= [w_1, \dots, w_D]; \quad D = (n + 1) \times q + (q + 1) \times m; \quad n = m = 4.\end{aligned}\quad (8)$$

The MLP neural scheme output represents the predictive output variable $y(k, \theta) = [y_1(k, \theta), y_2(k, \theta), y_3(k, \theta), y_4(k, \theta)]^T$ of weighting θ and regressive $\varphi(k)$ values. The real ZMP position $[x_{zmp_real}(k), y_{zmp_real}(k)]$ is determined using the forecast values $y(k, \theta)$ via WPG and ZMP equations.

It is clear to see that as to estimate the WPG for guaranteeing biped stepping stability, it needs to design the fitness function. The final object for humanoid robot is to achieve a stable stepping with respect to pre-chosen foot-lifting magnitude. Stable biped stepping is completely evaluated via the length from ZMP to biped support-foot center position during 1-step duration.

As to guarantee robot stable stepping under the desired ZMP trajectories regarding to pre-determined foot-raising value, it needs to design the fitness function. The robot stable stepping is verified based on the erroneous factor EN improved from the LMS value determined as follows,

$$E_{N1}(\theta) = \sum_{k=1}^N \left((x_{zmp_ref}(k) - x_{zmp_real}(k))^2 + (y_{zmp_ref}(k) - y_{zmp_real}(k))^2 \right), \quad (9)$$

where N represents the full sample number within one robot step.

Eq. (9) denotes the 1st fitness one. Moreover, another objective relates to robot to perfectly track the preset foot-lifting value – H_{ref} . Hence the residual of the real foot-lifting value with the preset one – H_{ref} , described at (10), is the 2nd fitness equation.

$$E_{N2}(\theta) = \sum_{k=1}^N (y_3(k) - H_{ref})^2. \quad (10)$$

Thus, in order to complete a stable and efficient robot walking met with desired ZMP trajectory and pre-determined foot-lifting magnitude, it requires to optimally minimize the two objective equations E_{N1} and E_{N2} . It forms eventually the objective function E_N (11) optimizing the following weight vector $\theta = [w_1, \dots, w_D]$.

$$E_N(\theta) = \lambda E_{N1}(\theta) + (1 - \lambda) E_{N2}(\theta) \quad (11)$$

In which, $\lambda(0 < \lambda < 1)$ represents an optimally chosen coefficient applied as to prior select either robust robot stepping (higher λ) or precise foot-lifting value (lower λ).

In this paper, the new enhanced EDE technique is applied. In the estimating phase, not only the desired ZMP $[x_{zmp_ref}(k), y_{zmp_ref}(k)]$ values but also the real ZMP $[x_{zmp_real}(k), y_{zmp_real}(k)]$ ones are optimally identified and thus the weight θ vector is adjusted.

3. PROPOSED EDE ALGORITHM FOR OPTIMAL WPG IMPLEMENTATION

The EDE technique is newly designed by modifying mutating factor F, along with control cross-over coefficient CR in exploration/exploitation of global optimum result. The full presentation of the enhanced EDE approach is improved from [21]. Below, the EDE technique is applied to optimally identify the weights of MLP neural model and

is fully presented in Table 1, in which GEN represents the maximum number of iterations; $\text{randint}(1, D)$ denotes the function that generates a value $\in [1 \div D]$. Moreover, it is important to choose the threshold value available which gives a critical effect on the global solution searching abilities of EDE algorithm. In case threshold value is too high compared of tolerance index, EDE shows a prior global searching; otherwise, in case threshold value shows too small, EDE tends to a prior in local searching. Thus, in order to select a best value regarding to the threshold, it needs to be dependent on the characteristics of user's problem. With this paper, the value of 10^{-3} is the best value chosen enable of efficiently balancing for not only exploration but also exploitation capabilities.

Table 1. Pseudo-code EDE algorithm training MLPNN

```

1 Begin
2 Generate randomly initialized population  $\theta_{i,G} = [w_{1,i,G}, w_{2,i,G}, \dots, w_{D,i,G}]$ 
3 Evaluate the fitness for each individual in population
4 for G=1 to GEN do
5   for i = 1 to NP do
6     jrand = randint(1, D)
7     CR = rand[0.7, 1.0]
8     F = rand[0.4, 1.0]
9     for j = 1 to D do
10      if rand[0,1] < CR or j = jrand then
11        if delta > threshold then
12          if rand > 0.3 then % using "rand/1"
13            Select randomly  $r_1 \neq r_2 \neq r_3 \neq i, \forall i \in \{1, 2, \dots, NP\}$ 
14             $u_{j,i,G+1} = w_{j,r_1,G} + F \times (w_{j,r_2,G} - w_{j,r_3,G})$ 
15          else % using "rand/2"
16            Select randomly  $r_1 \neq r_2 \neq r_3 \neq r_4 \neq r_5 \neq i, \forall i \in \{1, 2, \dots, NP\}$ 
17             $u_{j,i,G+1} = w_{j,r_1,G} + F \times (w_{j,r_2,G} - w_{j,r_3,G}) + F \times (w_{j,r_4,G} - w_{j,r_5,G})$ 
18          end if
19        else delta <= threshold
20          if rand > 0.3 then % using "best/1"
21            Select randomly  $r_1 \neq r_2 \neq best \neq i, \forall i \in \{1, 2, \dots, NP\}$ 
22             $u_{j,i,G+1} = w_{j,best,G} + F \times (w_{j,r_1,G} - w_{j,r_2,G})$ 
23          else % using "best/2"
24            Select randomly  $r_1 \neq r_2 \neq r_3 \neq r_4 \neq best \neq i, \forall i \in \{1, 2, \dots, NP\}$ 
25             $u_{j,i,G+1} = w_{j,best,G} + F \times (w_{j,r_1,G} - w_{j,r_2,G}) + F \times (w_{j,r_3,G} - w_{j,r_4,G})$ 
26          end if
27        end if
28      else
29         $u_{j,i,G+1} = w_{j,i,G}$ 
30      end if
31    end for
32    if  $E_N(U_{i,G+1}) \leq E_N(\theta_{i,G})$  then
33       $\theta_{i,G+1} = U_{i,G+1}$ 
34    else
35       $\theta_{i,G+1} = \theta_{i,G}$ 
36    end if
37  end for
38  delta =  $|(E_{N\_mean}/E_{N\_best}) - 1|$ 
39 end for
40 End

```

4. RESULTS AND ANALYSIS

The benefits of the proposed Neural-NARX model are analyzed in previous Sections. Here we present the full simulation plus experiment tests used to verifying applied to the small-sized experiment biped robot. Fig. 5 illustrates the biped architecture of the experiment biped robot. This small-sized biped includes 10 links whose mass are: $m_i = 70$ gam and $m_0 = 200$ gam. These links were designed to possess the following sizes (in cm): $d_1 = 5.6, d_2 = d_3 = 6, d_4 = 4, d_0 = 9, w = 6.3$.

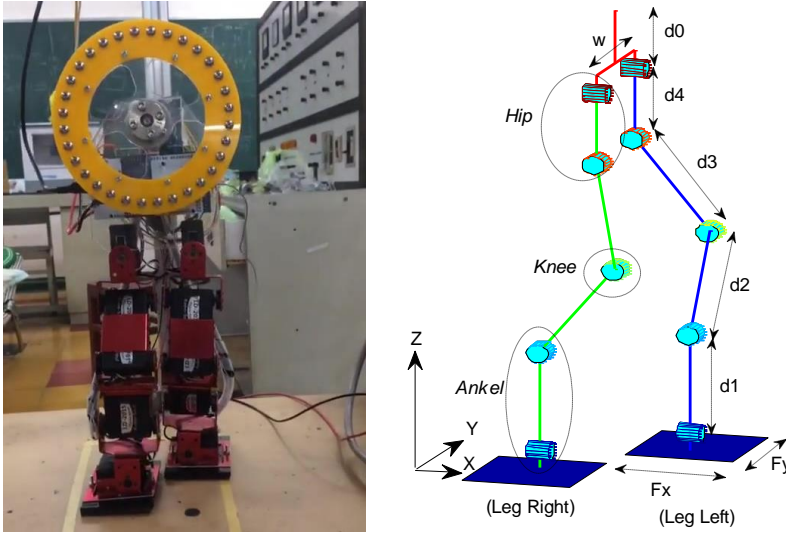


Fig. 5. The experiment biped robot structure

The desired biped ZMP trajectories are designed regarding to the constraint coefficients $X_{zmp_leave} = -1.2$ cm, $Y_{zmp_leave} = 0.9$ cm, $X_{zmp_land} = 1.6$ cm, $Y_{zmp_land} = 10$ cm, $S = 9.9$ cm, $T_c = 0.9$ s, $T_d = 0.5$ s and $T_s = 0.18$ s. Preset foot-raise value $H_{ref} = 1$ cm with λ in (11) selected equal 0.9. Coefficients of Neural-NARX scheme are optimally identified as: hidden node number $q = 8$, optimal sampled-step number in 1-cycle duration $N = 202$, the activating functions of neural model represent sigmoid ones.

4.1. EDE-based Neural-NARX Model Identification

The effectiveness of the suggested Neural-NARX is verified via benchmark-test of the humanoid robust stepping based on the desired biped ZMP trajectories and it validates the performance of the novel EDE algorithm through comparing the EDE with the traditional DE optimization method.

This case-study is started with initiated values and finally is to obtain the global optimal values in the seeking space. The swarm number is denoted as NP and the element dimension is represented as D in which contains all identified variables. Thus, the initial result is described as $\mathbf{W} = [\mathbf{W}_1, \mathbf{W}_2, \dots, \mathbf{W}_{NP}]^T$, where ' T ' is the transposed operator. Every component $\mathbf{W}_i (i = 1, 2, \dots, NP)$ is composed of $\mathbf{W}_i = [W_{i,1}, W_{i,2}, \dots, W_{i,D}]$. The appropriate approaches of each method are clarified here. It is necessary to notice that,

with respect to these techniques, the i index is changed within 1 to NP while the j one is changed within 1 up to D .

In this study, in order to equalize the exploration and exploitation balance of potential solutions collected with these two methods, each technique is evaluated via two thousand times. As a consequent, with these solutions realized about 10 runs, needed stochastic-based parameters, concerning the medium, the standardized residual, etc., required to be calculated for the comprehensive comparison. The NP number of two methods is selected equal 50 ($NP = 50$), Table 2 tabulates the DE and suggested EDE principal coefficients.

Table 2. Principal parameters of comparative optimization methods

Algorithm	Coefficients	Magnitude
DE	Mutant rate (F)	0.38
	Crossover rate (CR)	0.88
Proposed EDE	Threshold value	$1e-4$
	Mutant rate (F)	Hazard [0.3; 1.0]
	Crossover rate (CR)	Hazard [0.6; 1.0]

Exploiting all setting values above-mentioned, it is evident to notice that these selected parameters are successfully used in simulation. Consequently, these parameters are considered as “nominal magnitudes”. The flexibility of comparative optimization algorithms is verified based on such nominal magnitudes. Those optimization algorithms are all programmed in MATLAB version 2020b on HPE XL270d Gen10 Node CTO Server with 2*Intel Xeon-Silver 4216 (2.1GHz/16-core/100W) and 8*HPE 32GB (1x32GB) Dual Rank.

Table 3 presents the value of LMS (Least Mean Square) after each training procedure corresponding to two comparative optimization algorithms. After 10 training times of each optimal algorithm, the average value is also calculated and shown in this table. In Table 3, by comparing the value of LMS corresponding to each algorithm and results will be presented in Table 4. Moreover, Fig. 6 shows the convergent rate of LMS value in the estimating procedure. The dashed curve denotes the convergent velocity of each run meanwhile the bold curve shows the mean convergent rate from ten runs. The blue and red curves show the LMS convergent speed using the DE and the suggested EDE methods, respectively. In Fig. 7, it is easy to see the comparative ZMP trajectories of proposed Neural-NARX model response with the desired ZMP one. This apparently illustrates that the ZMP curve of Neural-NARX well tracks the desired ZMP curve and it always located within the biped support-foot area. That result ensures that the small-sized humanoid HUBOT-5 keeps stable stepping. Fig. 8 shows the comparison regarding to the response of robot 10 joint-angular values. Furthermore, the results shown in Fig. 6 confirm that the new EDE method quite better than the DE both in LMS accuracy and in convergence speed.

Table 3. Comparative LMS error values after training with 2 algorithms

Run	LMS of training Neural-NARX model (cm ²)	
	DE	Proposed EDE
1	544.568	332.307
2	353.814	353.814
3	436.233	332.134
4	343.809	334.724
5	368.244	332.480
6	406.201	342.878
7	680.712	333.311
8	361.987	332.442
9	540.523	336.210
10	379.065	390.073
Average	441.516	342.037

Table 4. The comparison of the LMS value corresponds to comparative algorithms

No	LMS of Training NARX-MLPNN model				
	Best (cm ²)	Worst (cm ²)	Mean (cm ²)	Variance (cm ²)	Time for 1 run (s)
DE	343.809	680.712	441.516	1.241e+04	17909.2135660000
EDE	332.134	390.073	342.037	3.318e+02	18479.5821080000

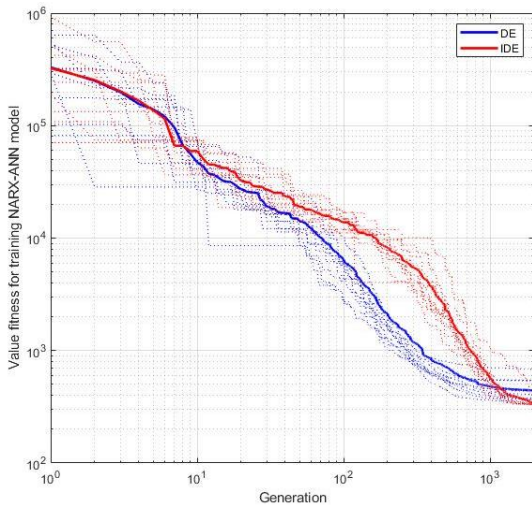


Fig. 6. The LMS convergent velocity in estimating procedure

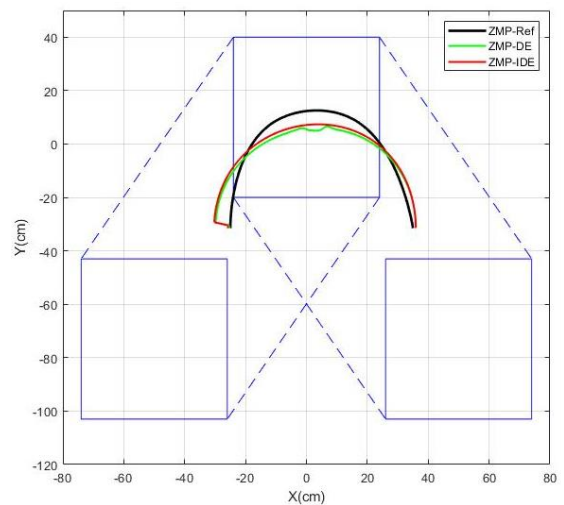


Fig. 7. Comparison between responded ZMP and reference ZMP trajectories

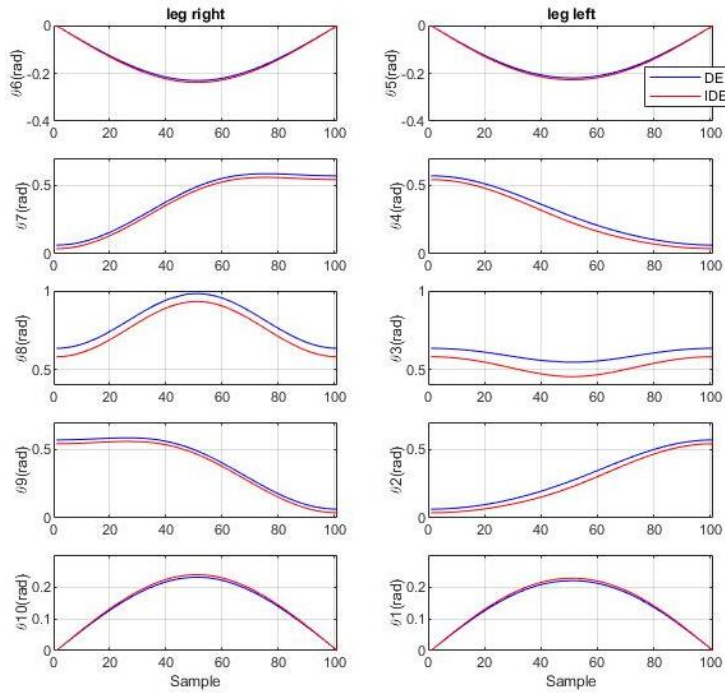


Fig. 8. Comparison between responded and reference biped ten rotating joint-angles

4.2. Simulation and experiment biped robust walking results

The 10 rotating joint-angle curves using the EDE approach are fully shown in Fig. 8 which confirm the simulated biped gait performance and strongly verify the robustness of HUBOT-5 walking as illustrated in Figs. 9 and 10.

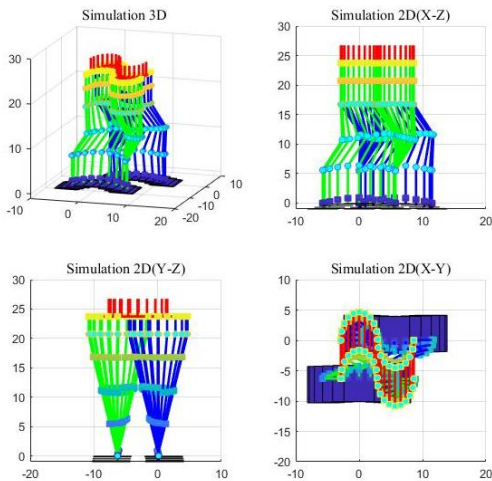


Fig. 9. Performance in gait simulation of humanoid HUBOT-5

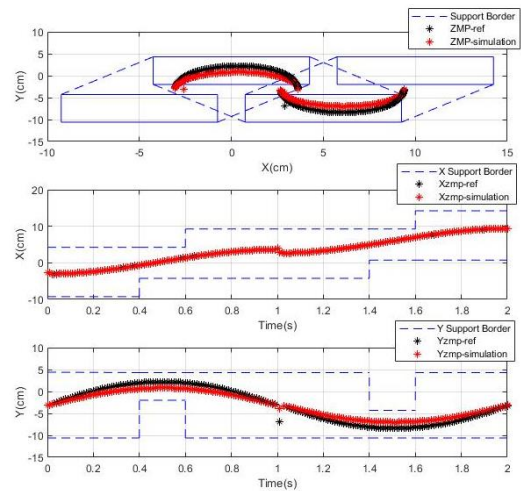


Fig. 10. Resulted ZMP trajectories

We continue applying the ten biped resulted joint-angle values to successfully regulate robust biped walking for the real small-sized HUBOT-5. Fig. 11 presents the photos of small-sized HUBOT-4 biped in realizing a one-step robust walking in terms of the desired foot-lift magnitude $H_{ref} = 1$ cm.

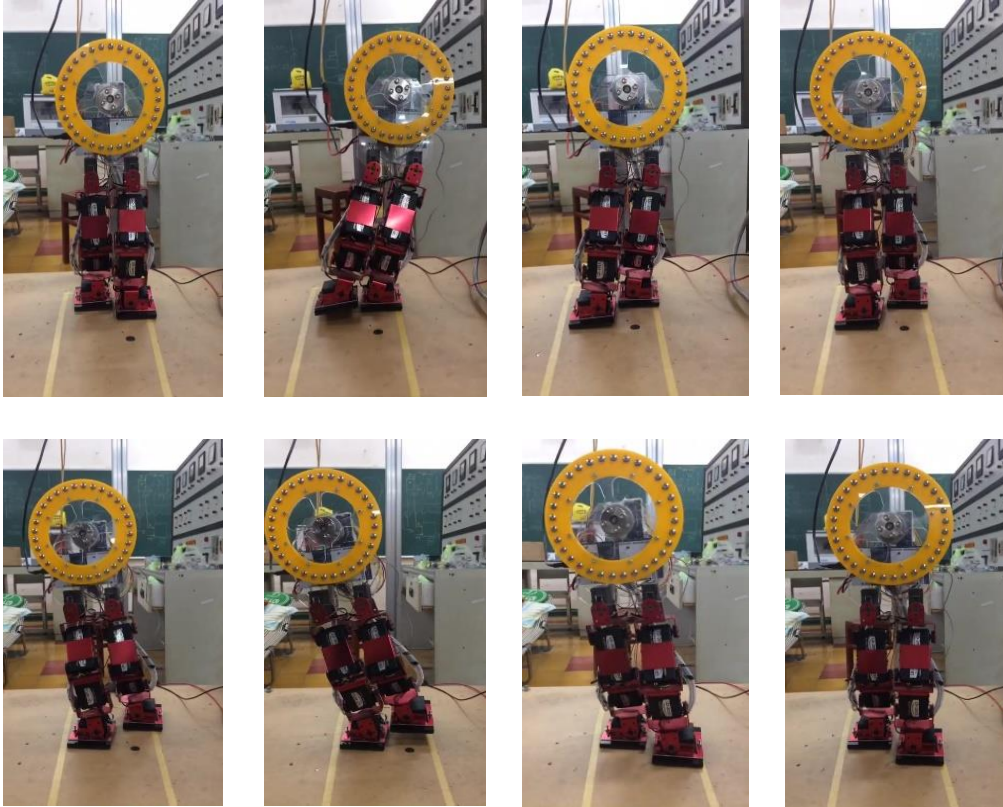


Fig. 11. Experiment HUBOT-5 biped realizing a one-step robust walking (with the desired foot-lift magnitude $H_{ref} = 1$ cm)

Developing the simulation results presented in Figs. 9 and 10, it leads the perfect experiment results illustrated in Figs. 11 and 12, which convincingly confirm that the investigation of pre-determined foot-lifting magnitude regarding to the task of well followed the desired ZMP trajectories along with the estimation for robust WPG generator. The proposed approach guarantees the HUBOT-5 to robust moving and holding step with pre-determined foot-lift value. The proposed technique for robust biped walking only using hybrid Neural-NARX model optimum estimated with enhanced EDE algorithm is convincingly enable. The optimized weights of NARX-MLPNN structure identified by EDE are tabulated in Table 5 which clearly presents that v_{ij} denotes the weights of hidden layer, in which i within 1 to 4, j from 1 to 8; b_h represents bias of hidden one; w_{ij} denotes the weights of output layer, in which i from 1 to 8, j from 1 to 4; b_0 is the output bias value.

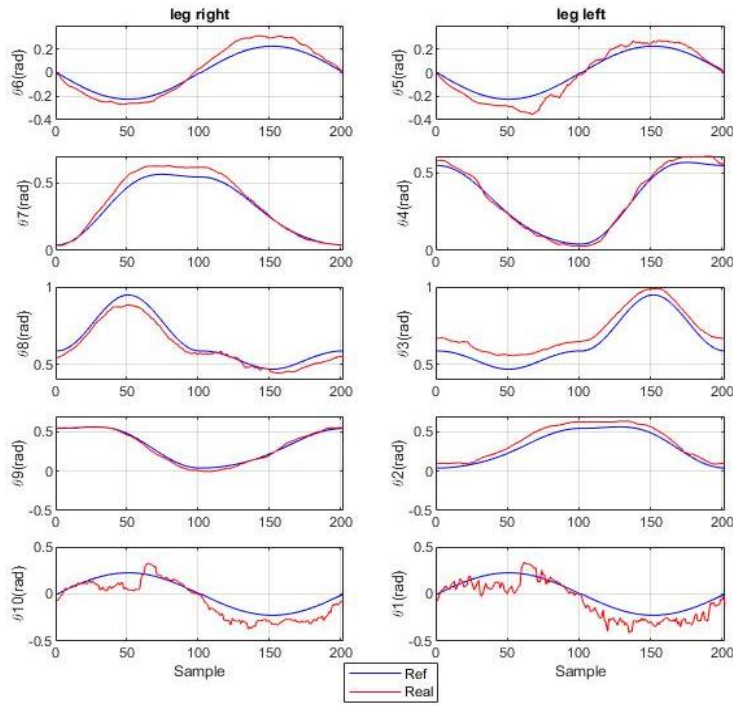


Fig. 12. Experiment ten one-step joint-angular trajectories of small-sized biped HUBOT-4

Table 5. The best optimized parameters of proposed Neural-NARX model trained by EDE

i	j								
	1	2	3	4	5	6	7	8	
v_{ij}	1	8.073	-9.295	9.129	9.684	10.676	-7.413	-6.026	-9.142
	2	-1.254	1.697	-2.411	-1.501	-5.090	0.216	1.359	-0.251
	3	-13.915	13.436	-11.240	-13.652	-12.959	13.956	10.256	13.697
	4	11.843	-10.579	12.652	11.077	13.143	-13.565	-12.417	-9.112
b_h	-8.803	16.067	-5.757	-0.286	11.228	-13.738	13.197	-17.288	
w_{ij}	1	-12.489	2.308	-6.216	-14.537				
	2	12.470	-1.260	-11.558	7.235				
	3	-12.302	-12.488	-7.976	-9.887				
	4	-14.280	9.119	0.915	-13.703				
	5	-12.544	1.818	-12.071	-9.930				
	6	13.465	-6.578	-3.327	-0.474				
	7	10.497	10.251	13.682	10.835				
	8	12.987	4.780	-8.028	-4.887				
b_0	13.843	3.568	-7.441	-12.884					

5. CONCLUSIONS

This paper introduces a new WPG for robust humanoid stepping regarding to desired ZMP reference along with pre-determined foot-lift value. This paper's key contributions are to be concisely cited as. A new planning technique for the desired biped ZMP trajectory is innovatively proposed. A new biped WPG generator is introduced using the proposed Neural-NARX scheme and optimized by enhanced EDE technique. Eventually the biped WPG is successfully implemented in the real small-sized HUBOT-5 biped robot. Both of simulating and experimenting results confirm that the real small-sized HUBOT-5 robot can stably step regarding to versatile desired ZMP trajectories and efficiently keep pace with pre-determined foot-lift value. The suggested methods of the study show quite original compared of the other latest and modern techniques on biped WPG proposed in recent years.

DECLARATION OF COMPETING INTEREST

The authors declare that they have no known competing financial interests or personal relationships that could have appeared to influence the work reported in this paper.

ACKNOWLEDGMENT

We acknowledge Ho Chi Minh City University of Technology (HCMUT), VNU-HCM for supporting this study.

This research is funded by Vietnam National University Ho Chi Minh City (VNU-HCM) under grant number DS2022-20-09.

REFERENCES

- [1] C. Chevallereau, G. Bessonnet, G. Abba, and Y. Aoustin. *Bipedal robots: Modeling, design and walking synthesis*. Wiley, (2008). <https://doi.org/10.1002/9780470611623>.
- [2] M. Vukobratovic and B. Borovac. Zero-moment point - Thirty five years of its life. *International Journal of Humanoid Robotics*, **01**, (2004), pp. 157–173. <https://doi.org/10.1142/s0219843604000083>.
- [3] E. Ohashi, T. Sato, and K. Ohnishi. A walking stabilization method based on environmental modes on each foot for biped robot. *IEEE Transactions on Industrial Electronics*, **56**, (2009), pp. 3964–3974. <https://doi.org/10.1109/tie.2009.2024098>.
- [4] J. Yi, Q. Zhu, R. Xiong, and J. Wu. Walking algorithm of humanoid robot on uneven terrain with terrain estimation. *International Journal of Advanced Robotic Systems*, **13**, (2016). <https://doi.org/10.5772/62245>.
- [5] C. Liu, J. Ning, and Q. Chen. Dynamic walking control of humanoid robots combining linear inverted pendulum mode with parameter optimization. *International Journal of Advanced Robotic Systems*, **15**, (2018). <https://doi.org/10.1177/1729881417749672>.
- [6] S. Liu and P. Liu. Benchmarking and optimization of robot motion planning with motion planning pipeline. *The International Journal of Advanced Manufacturing Technology*, **118**, (2021), pp. 949–961. <https://doi.org/10.1007/s00170-021-07985-5>.
- [7] Y. Meng, S. Kuppannagari, and V. Prasanna. Accelerating proximal policy optimization on CPU-FPGA heterogeneous platforms. In *Proceeding of IEEE 28th Annual International Symposium on Field-Programmable Custom Computing Machines (FCCM)*, Piscataway, IEEE, (2020), pp. 19–27, <https://doi.org/10.1109/FCCM48280.2020.00012>.

- [8] T. T. Huan, C. V. Kien, H. P. H. Anh, and N. T. Nam. Adaptive gait generation for humanoid robot using evolutionary neural model optimized with modified differential evolution technique. *Neurocomputing*, **320**, (2018), pp. 112–120. <https://doi.org/10.1016/j.neucom.2018.08.074>.
- [9] V.-H. Dau, C.-M. Chew, and A.-N. Poo. Optimal trajectory generation for bipedal robots. In *Proceeding of 7th IEEE-RAS International Conference on Humanoid Robots*, Pittsburgh, PA, USA, IEEE, (2007), pp. 603–608.
- [10] S. Wang, W. Chaovalitwongse, and R. Babuska. Machine learning algorithms in bipedal robot control. *IEEE Transactions on Systems, Man, and Cybernetics, Part C (Applications and Reviews)*, **42**, (2012), pp. 728–743. <https://doi.org/10.1109/tsmcc.2012.2186565>.
- [11] S. Phaniteja, P. Dewangan, P. Guhan, A. Sarkar, and K. M. Krishna. A deep reinforcement learning approach for dynamically stable inverse kinematics of humanoid robots. In *Proceeding of IEEE International Conference on Robotics and Biomimetics (ROBIO)*, IEEE, (2017), <https://doi.org/10.1109/robio.2017.8324682>.
- [12] N. Navarro-Guerrero, C. Weber, P. Schroeter, and S. Wermter. Real-world reinforcement learning for autonomous humanoid robot docking. *Robotics and Autonomous Systems*, **60**, (2012), pp. 1400–1407. <https://doi.org/10.1016/j.robot.2012.05.019>.
- [13] K.-S. Hwang, W.-C. Jiang, Y.-J. Chen, and H. Shi. Motion segmentation and balancing for a biped robot's imitation learning. *IEEE Transactions on Industrial Informatics*, **13**, (2017), pp. 1099–1108. <https://doi.org/10.1109/tii.2017.2647993>.
- [14] H. Kim, D. Seo, and D. Kim. Push recovery control for humanoid robot using reinforcement learning. In *Proceeding of 2019 Third IEEE International Conference on Robotic Computing (IRC)*, IEEE, (2019). <https://doi.org/10.1109/irc.2019.00102>.
- [15] C. Gil, H. Calvo, and H. Sossa. Learning an efficient gait cycle of a biped robot based on reinforcement learning and artificial neural networks. *Applied Sciences*, **9**, (2019). <https://doi.org/10.3390/app9030502>.
- [16] A. Xi and C. Chen. Walking control of a biped robot on static and rotating platforms based on hybrid reinforcement learning. *IEEE Access*, **8**, (2020), pp. 148411–148424. <https://doi.org/10.1109/access.2020.3015506>.
- [17] W. Zhang, Y. Jiang, F. U. D. Farrukh, C. Zhang, D. Zhang, and G. Wang. LORM: a novel reinforcement learning framework for biped gait control. *PeerJ Computer Science*, **8**, (2022). <https://doi.org/10.7717/peerj-cs.927>.
- [18] T. T. Huan and H. P. H. Anh. Comparative stable walking gait optimization for small-sized biped robot using meta-heuristic optimization algorithms. *Vietnam Journal of Mechanics*, **40**, (2018), pp. 407–424. <https://doi.org/10.15625/0866-7136/12294>.
- [19] Q. Huang, K. Yokoi, S. Kajita, K. Kaneko, H. Arai, N. Koyachi, and K. Tanie. Planning walking patterns for a biped robot. *IEEE Transactions on Robotics and Automation*, **17**, (2001), pp. 280–289. <https://doi.org/10.1109/70.938385>.
- [20] G. Dip, V. Prahlaad, and P. D. Kien. Genetic algorithm-based optimal bipedal walking gait synthesis considering tradeoff between stability margin and speed. *Robotica*, **27**, (2009), pp. 355–365. <https://doi.org/10.1017/s026357470800475x>.
- [21] T. T. Thong, T. T. Huan, C. V. Kien, and H. P. H. Anh. An advanced fuzzy control for maximum power point tracking PV system optimized with modified MDE algorithm. In *Proceeding of 2021 International Conference on System Science and Engineering (ICSSE)*, IEEE, (2021), <https://doi.org/10.1109/icsse52999.2021.9538458>.